DOI: 10.1002/ejic.201000038

Monazite and Zircon Type $LaVO_4$:Eu Nanocrystals – Synthesis, Luminescent Properties, and Spectroscopic Identification of the Eu^{3+} Sites

Chun-Jiang Jia,[a] Ling-Dong Sun,*[a] Zheng-Guang Yan,[a] Yu-Cheng Pang,[a] Shao-Zhe Lü,[b] and Chun-Hua Yan*[a]

Keywords: Rare earths / Nanocrystals / Vanadates / Europium / Doping / Luminescence

Pure monoclinic- (m) and tetragonal (t) $LaVO_4$:Eu nanocrystals were prepared by a facile citric anion- and EDTA (ethylenediaminetetraacetic acid)-assisted hydrothermal method, respectively. The structure is characterized by XRD, Raman spectroscopy, and electron microscopy. Besides structure characterization, site-selective emission spectroscopy was used to investigate the relationship between the microstructure and luminescent characters of the m- and t-$LaVO_4$:Eu nanocrystals. The results show that for both the m- and t-$LaVO_4$:Eu nanocrystals, the Eu^{3+} ions occupy two types of sites, one that is the same as that of the corresponding bulk and the other that is specific to the surface states of the nanocrystals. These investigations not only provide important experimental evidence for rare earth luminescence studies, but also disclose the correlation between the microstructure and luminescence behavior, which could be used as a guide to the design and synthesis of novel luminescence materials. It is also shown that t-$LaVO_4$:Eu is a promising luminescence material with a high quantum yield and low cost.

Introduction

Rare-earth-doped luminescence materials have been extensively studied in the past few decades because of their wide application in lighting,[1] displays,[2] lasers,[3] and amplifiers for fiber-optic communication.[4] Recently, studies also disclose their potential application in biological detection and biotechnology.[5] This inspires research on rare-earth-doped luminescence nanocrystals, both in terms of synthesis and size and structure-dependent luminescence behavior.

For rare-earth–ion-activated luminescence materials, yttrium-based lattices, such as Y_2O_3,[6] YBO_3,[7] YVO_4[8] amongst others, are usually used as hosts because of their suitable crystal structure and high chemical stability. In comparison with Y, La is more abundant in rare earth mineral resources and La_2O_3 is much cheaper than Y_2O_3. However, the development of La-based materials is still inadequate and La_2O_3 is overstocked in the rare earth industry. It is valuable to fundamentally and practically study the La-based materials for the balanced-utilization of the rare earth natural resources. Unlike the other members of the rare earth family, such as Y, Gd, and Lu, La-based luminescence materials do not exhibit good performance because it is structurally different. The larger radius results in a higher coordination number and a low symmetrical crystal structure for La compounds, and this prohibits their application as luminescence host materials. It is therefore very important to attempt to obtain the desired structured La-based materials and study their luminescence properties for both scientific research and practical applications.

Among the rare-earth-functional materials, lanthanide orthovanadate is an important family and has attracted great interest because of their various technological applications in catalysts,[9] polarizers,[10] laser host materials,[3] and phosphors.[11] The lanthanide orthovanadates crystallize in two phases, namely, a tetragonal phase (t-) with a zircon structure[12] and a monoclinic phase (m-) with a monazite structure.[13] Generally, the larger Ln^{3+} ion prefers the monazite structure owing to its higher oxygen coordination number of 9 compared to 8 of the zircon type. Therefore, $LaVO_4$ crystallizes solely as the monazite type in an equilibrium state and other orthovanadates including those of Sc and Y crystallize as the zircon type.[14] In addition to the thermodynamically stable monazite structure, $LaVO_4$ can also crystallize as the zircon structure,[15–17] a metastable polymorph, under some mild conditions. Therefore, Eu^{3+}-doped $LaVO_4$ can be formed as either the monazite- or zircon type of structure. Although m-$LaVO_4$ was not regarded as a good host for Eu^{3+} ions, t-$LaVO_4$:Eu may be a promising luminescence material because of its zircon structure, similar to that of YVO_4:Eu. Therefore, among the rare-

[a] Beijing National Laboratory for Molecular Sciences, State Key Laboratory of Rare Earth Materials Chemistry and Applications, PKU-HKU Joint Laboratory in Rare Earth Materials and Bioinorganic Chemistry, Peking University,
Beijing 100871, China
Fax: +86-01-62754179
E-mail: yan@pku.edu.cn
[b] Open Laboratory of Excited States, Chinese Academy of Sciences,
Changchun 130021, China

Supporting information for this article is available on the WWW under http://dx.doi.org/10.1002/ejic.201000038.

earth-ion-activated Ln-based luminescence materials, $LaVO_4$:Eu was chosen as it has two crystal phases (monazite and zircon) and it can be selectively investigated for its structure-related properties on the nanometer scale. There have been some reports on $LaVO_4$:Eu nanocrystals;[11,17–23] however, luminescence studies of both m- and t-$LaVO_4$:Eu nanocrystals are still limited.

In our previous work,[18] we found that only bulk m-$LaVO_4$:Eu with low Eu^{3+} content (≤3 mol-%) can be prepared by solid-state reaction because of the different structures of m-$LaVO_4$ (monazite structure) and $EuVO_4$ (zircon structure), while the metastable t-$LaVO_4$:Eu cannot be formed, which confines the studies on $LaVO_4$:Eu. Relative to the traditional solid-state reaction method, the solution route synthesis, a relatively mild method, has proven to be effective and convenient in structure selectivity at low temperature on a large scale. Although it is hard to systematically study the luminescence behavior of bulk m- and t-$LaVO_4$:Eu owing to the limitation on structure control with the solid-state reaction, there is still a great possibility of investigating the structure and properties of nanostructured $LaVO_4$:Eu. In this paper, pure m- and t-$La_{1-x}VO_4$:Eu_x ($0 < x \leq 0.20$) nanocrystals were selectively synthesized by a facile hydrothermal method and their luminescence properties were studied. Relative to the m-$LaVO_4$:Eu nanocrystals, the luminescence behavior of the t-$LaVO_4$:Eu nanocrystals was greatly improved because of their zircon structure, which provides a new and cheap candidate for luminescence materials with wide potential applications in lighting, displays, and biological detection.

In order to further explore the correlation between microstructure and luminescence behavior of the m- and t-$LaVO_4$:Eu nanocrystals, spectroscopic identification of the Eu^{3+} sites in the nanocrystals was carried out by site-selective emission spectroscopy. In both m- and t-$LaVO_4$:Eu nanocrystals, the Eu^{3+} ions occupy two types of sites, one that is the same as that of bulk monazite $LaVO_4$ or zircon $YVO_4$and the other that is a specific to Eu^{3+} located at the surfaces of the nanocrystals. A detailed study of the site-selective emission spectra for the $LaVO_4$:Eu nanocrystals not only provides important evidence for the structure-related intraconfigurational $4f^N$–$4f^N$ transitions, but also discloses the importance of the microstructure on the luminescence properties, which could be applied to guide the design and synthesis of novel luminescent materials.

Results and Discussion

Synthesis and Structure Characterization of the m- and t-$LaVO_4$:Eu Nanocrystals

m-$LaVO_4$:Eu Nanocrystals

m-$LaVO_4$:Eu nanocrystals were prepared with $La(NO_3)_3$, $Eu(NO_3)_3$, Na_3VO_4, and sodium citrate as starting materials by hydrothermal treatment at 180 °C for 24 h. Sodium citrate is important for obtaining pure stuctured m-$LaVO_4$:Eu nanocrystals. The ratio of Eu/(Eu+La) was varied from 0 to 0.20, and at higher ratios, phase transition from monozite to zircon and phase segregation take place. The XRD patterns of the m-$LaVO_4$:Eu nanocrystals are shown in Figure 1. When the initial molar ratio of Eu/(Eu+La) is lower than 0.20, all the diffraction peaks are well indexed relative to those of the standard m-$LaVO_4$ sample (JCPDS card No. 50–0367) without traces of other phases. The citric ions play a crucial role in the formation of pure m-$LaVO_4$:Eu nanocrystals. In comparison with m-$LaVO_4$, $EuVO_4$ tends to crystallize as the zircon-type structure because of the smaller radius of Eu^{3+}; therefore, the directly fast reaction between La^{3+}/Eu^{3+} and VO_4^{3-} induces the formation of m-$LaVO_4$ and $EuVO_4$ nanocrystals, instead of m-$LaVO_4$:Eu. For the as-prepared m-$La_{1-x}VO_4$:Eu_x ($x \leq 0.2$) nanocrystals, the least-squares refined crystallographic parameters were obtained by using the software "LAPOD", as listed in Table S1. The radius of Eu^{3+} (112 pm,[24] with oxygen coordination number of 9) is smaller than that of La^{3+} (121.6 pm,[24] with oxygen coordination number of 9); therefore, a linear decrease in the unit cell parameters (Figure S1) is observed with an increase in the Eu content, which indicates that the Eu^{3+} ions have entered the lattice of the m-$LaVO_4$ nanocrystals by substituting the La^{3+} ions.

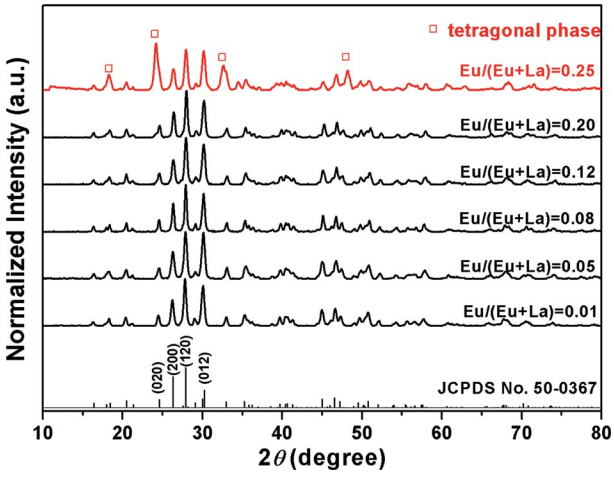

Figure 1. XRD patterns of the m-$LaVO_4$:Eu nanocrystals. Tetragonal-phased $EuVO_4$ crystallizes separately as the molar ratio of Eu/(Eu+La) is increased above 0.20.

The phase purity of the as-prepared m-$LaVO_4$:Eu nanocrystals is also confirmed by Raman spectroscopy. Figure 2 shows the Raman spectra of the pure $EuVO_4$ and m-$La_{1-x}VO_4$:Eu_x (x = 0, 0.05, 0.10, and 0.20) nanocrystals. The spectra comprises two parts, namely, the peaks at high energy between 745 and 880 cm^{-1}, which corresponds to the "internal" vibrations of the tetrahedral VO_4^{3-} group, and the peaks below 475 cm^{-1}, which mainly originate from the La–O vibrations.[17,20] Both the low-energy and high-energy region of the Raman spectra shown in Figure 2b–d are the same as those of the pure m-$LaVO_4$ nanocrystals (Figure 2a). For comparison, pure $EuVO_4$ nanocrystals were also prepared, the XRD pattern and TEM image of which are shown in Figure S2. The Raman spectra of m-

$LaVO_4$:Eu (Figure 2b–d) nanocrystals differ greatly from that of the pure $EuVO_4$ nanocrystals (Figure 2e), which confirms that Eu^{3+} ions effectively enter the lattice of the host (m-$LaVO_4$) by replacing La^{3+} ions. These results are consistent with those of the above XRD analysis.

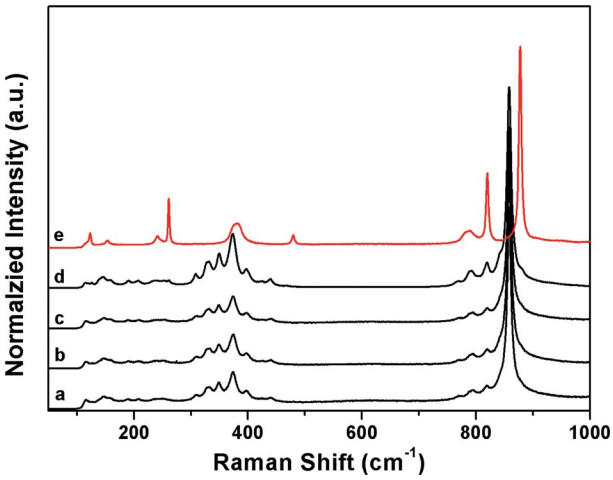

Figure 2. Raman spectra of the as-prepared m-$La_{1-x}VO_4$:Eu_x (a–d) and $EuVO_4$ (e) nanocrystals: (a) x = 0, (b) x = 0.05, (c) x = 0.10, and (d) x = 0.20.

The TEM and HRTEM images of the as-prepared m-$LaVO_4$:Eu nanocrystals are shown in Figure 3. The m-$LaVO_4$:Eu nanocrystals crystallize well, with a diameter range from 30 to 50 nm (Figure 3a). The clear lattice fringe and well-evolved facets shown in Figure 3b also suggest the single-crystal nature of the m-$LaVO_4$:Eu polyhedron nanocrystals.

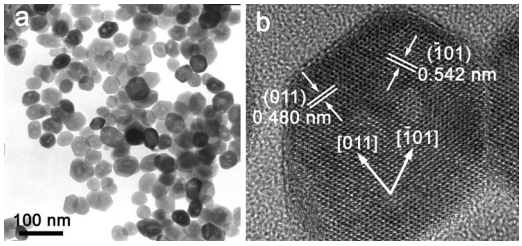

Figure 3. (a) TEM and (b) HRTEM images of the m-$LaVO_4$:Eu nanocrystals.

t-$LaVO_4$:Eu Nanocrystals

In our previous work, it was found that chelating ligands, such as EDTA, favor the formation of t-$LaVO_4$ through a solution approach.[17] Here, pure t-$LaVO_4$:Eu nanocrystals were synthesized by an EDTA-assisted hydrothermal method. The structure and morphology of the samples are characterized with XRD, Raman spectroscopy, and electron microscopy. The XRD patterns of the t-$LaVO_4$:Eu nanocrystals are shown in Figure 4. All the peaks are well indexed to the standard t-$LaVO_4$. The least-squares refined crystallographic parameters were also obtained by using the software "LAPOD", as listed in Table S2. The unit cell parameters (Figure S3) decrease linearly with an increase in the Eu content, which confirms the effective doping by Eu^{3+} ions in the lattice of the host t-$LaVO_4$.

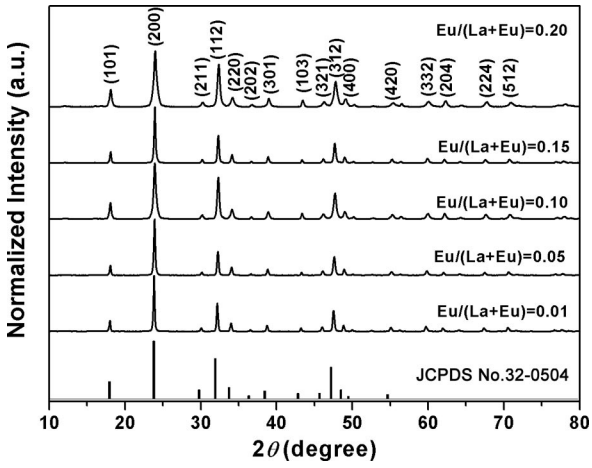

Figure 4. XRD patterns of the t-$LaVO_4$:Eu nanocrystals.

The Raman spectra of t-$La_{1-x}VO_4$:Eu_x (x = 0.01, 0.05, 0.10, 0.15, 0.20) are shown in Figure 5. Because of the different structures, the Raman spectra of the t-$LaVO_4$:Eu nanocrystals, especially the peaks in the low-energy region that correspond to La–O vibrations (below 475 cm^{-1}), are quite different from those of m-$LaVO_4$:Eu shown in Figure 2. The lower coordination number (8) and the high symmetry (D_{2d}) of the La^{3+}/Eu^{3+} ions contribute to the relatively simple vibration modes in comparison with those of m-$LaVO_4$:Eu.[17,20] Comparison of the Raman spectra of the t-$La_{1-x}VO_4$:Eu_x nanocrystals (Figure 5a–e) with that of pure $EuVO_4$ nanocrystals (Figure 5f), it is clear that $EuVO_4$ does not form separately from the t-$La_{1-x}VO_4$:Eu_x nanocrystals.

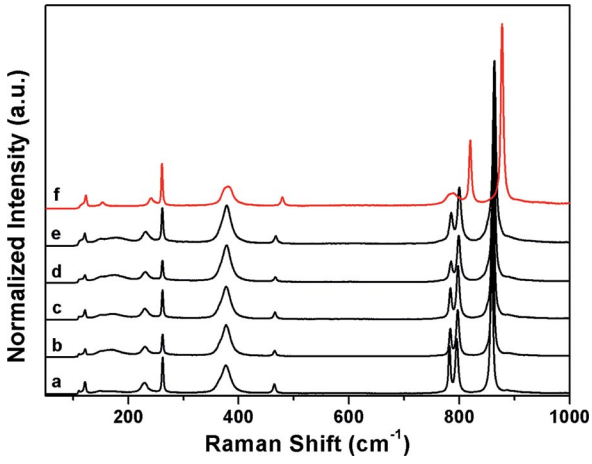

Figure 5. Raman spectra of the as-prepared t-$La_{1-x}VO_4$:Eu_x (a–e) and $EuVO_4$ (f) nanocrystals: (a) x = 0.01, (b) x = 0.05, (c) x = 0.10, (d) x = 0.15, and (e) x = 0.20.

Figure 6 shows the TEM and HRTEM images of the as-prepared t-$LaVO_4$:Eu nanocrystals. The products are composed of rodlike nanocrystals with a diameter of 10–15 nm

and length of 150–250 nm. The HRTEM image (Figure 6b) presents a single crystalline nanorod with a growth direction of [001].

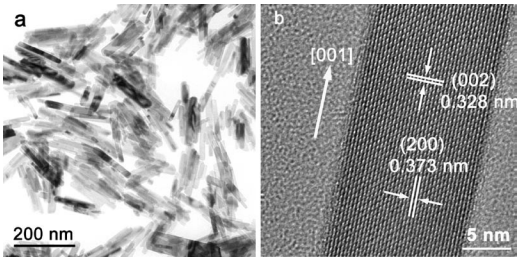

Figure 6. (a) TEM and (b) HRTEM images of the t-$LaVO_4$:Eu nanocrystals.

Bulk $LaVO_4$:Eu

For comparison, bulk $LaVO_4$:Eu was prepared by a direct solid-state reaction method. The XRD patterns of the as-prepared bulk $La_{1-x}VO_4:Eu_x$ are shown in Figure S4. It can be seen that when $x > 0.03$, traces of the zircon-type structure appear, which indicates that pure bulk m-$LaVO_4$:Eu can be obtained only with very low molar ratio of Eu/(Eu+La) ($\leq$0.03). At higher temperatures, $LaVO_4$ tends to crystallize in its thermodynamically stable phase, as the monazite-type structure, while $EuVO_4$ crystallizes as the zircon–type structure. Because of the difference in structure between m-$LaVO_4$ and $EuVO_4$ and the diffusion limitation in the solid-state reaction, bulk m-$LaVO_4$:Eu with high Eu content is difficult to form. t-$LaVO_4$ is metastable and will transform into m-$LaVO_4$ at high temperature, therefore bulk t-$LaVO_4$:Eu could not be prepared by the solid-state reaction method.

Luminescent Properties of m- and t-$LaVO_4$:Eu Nanocrystals

m-$LaVO_4$:Eu Nanocrystals

Figure 7 depicts the emission spectra of the m-$La_{1-x}VO_4:Eu_x$ (x = 0.03) nanocrystals and the corresponding bulk material excited at 310 nm (Xe lamp). These spectra are similar with respect to both the position and number of emission peaks in the range 580–720 nm, which arise from the $^5D_0$–^7F_J transitions (J = 0, 1, 2, 3, 4) of the Eu^{3+} activator. The most intense emission at 600–630 nm originates from the partially allowed $^5D_0$–$^7F_2$ electric-dipole transition, which becomes dominant in the absence of an inversion center (C_1 symmetry) as disclosed by the Judd–Ofelt theory.[25,26] The excitation spectrum (Figure 7b) can be divided into two regions. The first corresponds well to the absorption of the vanadate group at wavelengths below 350 nm, which indicates that the emission in Figure 7a results from energy transfer from the vanadate groups to the excited states of europium ions. The second region encompasses the 4f absorption of the europium ions at 396 and 467 nm. The latter absorptions are much weaker because of the low absorption cross section and the forbidden character of the 4f transitions. Furthermore, the excitation in this region is rather inefficient relative to that of the vanadate groups.

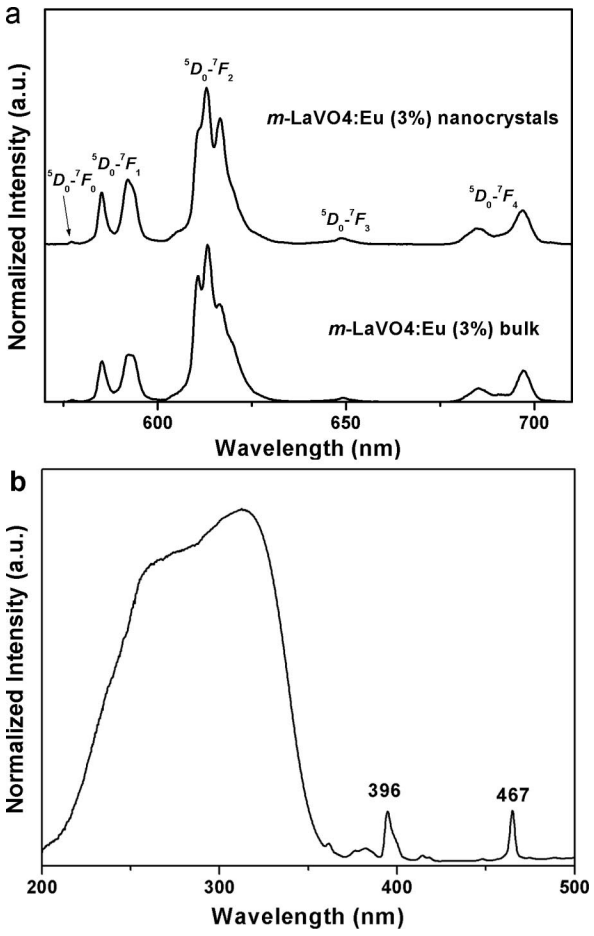

Figure 7. (a) Emission spectra of the m-$LaVO_4$:Eu (3 mol-%) nanocrystals and of the bulk excited at 310 nm (Xe lamp). (b) Excitation spectrum of the m-$LaVO_4$:Eu (3 mol-%) nanocrystals.

The relationship between the emission intensity and dopant content of bulk and nanosized m-$LaVO_4$:Eu is shown in Figure 8. For the bulk material, with an increase in the Eu content from 1 to 3 mol-%, the emission intensity increases linearly. But the quenching concentration, an important parameter for luminescent materials with activators, cannot be determined since it is impossible to get pure bulk m-$LaVO_4$:Eu when the Eu content is higher than 0.03. As for commonly studied Eu^{3+}-doped phosphors, Y_2O_3:Eu and YVO_4:Eu, the quenching concentration is ca. 5%, while it increases to ca. 12% for the m-$LaVO_4$:Eu nanocrystals (the squares in Figure 8). This phenomenon has also been observed in other systems, such as YBO_3:Eu nanocrystals.[27] The deficiency of traps, which results from the limited primitive cells per particle, as well as the hindrance of energy transfer from the particle boundaries should be responsible for the increased quenching concentration with decreasing particle size, as discussed in the literature.[27]

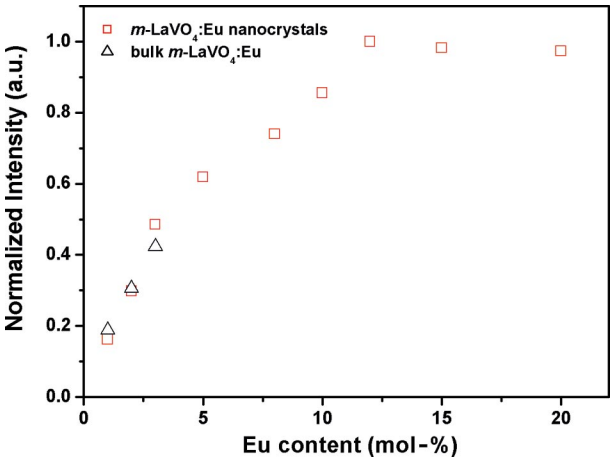

Figure 8. Integrated emission intensity vs. Eu content of the m-$LaVO_4$:Eu nanocrystals and the bulk material. The intensity values are normalized with that of the m-$LaVO_4$:Eu (12 mol-%) nanocrystals.

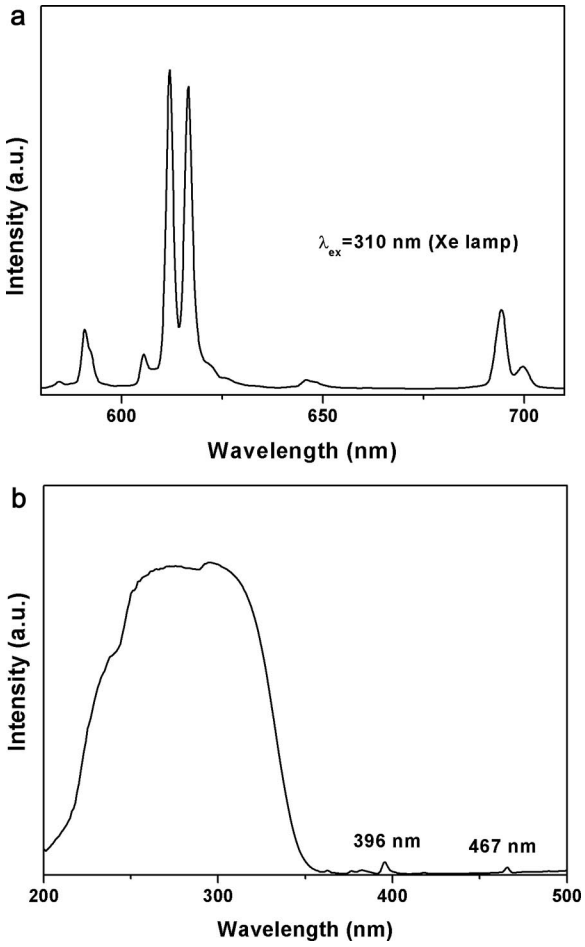

Figure 9. (a) Emission spectra of the t-$LaVO_4$:Eu (10 mol-%) nanocrystals excited at 310 nm (Xe lamp). (b) Excitation spectra of the t-$LaVO_4$:Eu (10 mol-%) nanocrystals.

t-$LaVO_4$:Eu Nanocrystals

Figure 9a,b show the emission and excitation spectra of the t-$LaVO_4$:Eu (10 mol-%) nanocrystals. The emission spectrum is similar in position but different in transition branch ratio to that of m-$LaVO_4$:Eu. The spectral splitting, which comes from the Stark effect of different crystal fields with various crystal structure, are quite different for t- and m-$LaVO_4$:Eu. In order to get a full view of the luminescence behavior of the m- and t-$LaVO_4$:Eu nanocrystals, and in addition to the luminescence spectra, the quantum yields of both types of nanocrystals have been carefully measured at room temperature. It is deduced that m-$LaVO_4$:Eu (12 mol-%) and t-$LaVO_4$:Eu (10 mol-%) nanocrystals exhibit the highest quantum yields, 19% and 65%, respectively, among the corresponding nanocrystals as determined by reference with a Rhodamine B ethanol solution with an optical density (OD) of less than 0.1 and excitation at 310 nm.

It is important to understand the reason behind the great difference between the emission efficiency of the m- and t-$LaVO_4$:Eu nanocrystals for research and application purposes. On the basis of the Stark energy levels under different crystal fields, this difference in emission efficiency mainly originates from the difference in structure of the host, which directly affects the transition and recombination process. For Eu^{3+}-doped phosphors, the structure of the host is a very important factor that determines the emission efficiency. As discussed for Eu^{3+}-doped lanthanide orthovanadates,[28,29] almost all of the energy transfer through VO_4^{3-}–VO_4^{3-}, VO_4^{3-}–Eu^{3+}, and Eu^{3+}–Eu^{3+} occur after the absorption of photons. These transfer processes are all the more favored when there is greater overlap of the wave functions. Therefore, the difference in the luminescence behavior of m- and t-$LaVO_4$:Eu lies in the fact that the energy transfer based on the exchange interaction is more efficient in t-$LaVO_4$:Eu than in m-$LaVO_4$:Eu. In fact, a necessary condition for this mechanism is the overlap of the wave functions of the vanadium and lanthanum (europium) centers. In t-$LaVO_4$:Eu, for each lanthanum or europium center, there are four bond bridges of La/Eu–O–V with a maximum angle of 153° (Figure 10a), which makes the σ bonding overlap effectively, therefore the energy transfer in t-LaVO4:Eu is greatly improved. While in m-$LaVO_4$:Eu, for one lanthanum (europium) center, there is only one La/Eu–O–V bond bridge with an angle of 153°, the other La/Eu–O–V bond bridge angles are much smaller (Figure 10b), so that the possibilities of an exchange interaction are drastically reduced and the effective energy transfer cannot occur. The structural transformation of $LaVO_4$ from the monazite- to the zircon-type structure greatly improves the quantum yield and emission intensity of $LaVO_4$:Eu. Considering the low cost of commercial La-based raw materials, t-$LaVO_4$:Eu may be a promising luminescence material candidate for red phosphors and has a potential use as a biological detector.

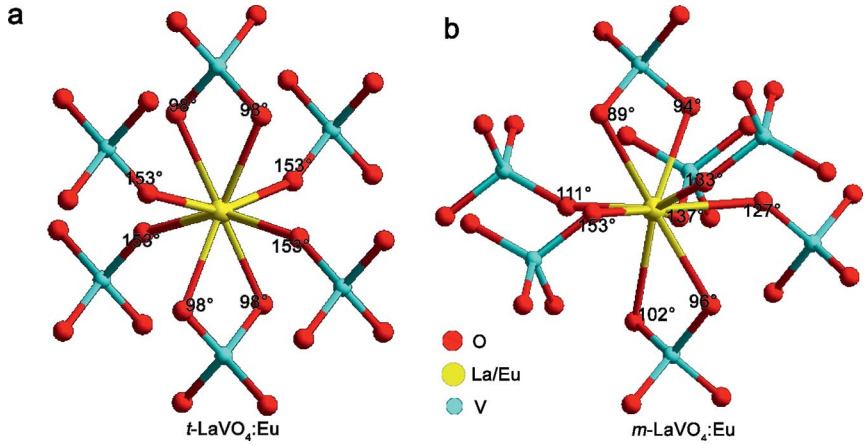

Figure 10. Simulated crystal structure of (a) t- and (b) m-$LaVO_4$:Eu.

Spectroscopic Identification of the Eu^{3+} Sites in m- and t-$LaVO_4$:Eu Nanocrystals

For rare-earth-doped materials, the local environment of the dopant ions is believed to have a crucial impact on the luminescence behavior and it is important to distinguish between the contributions from the sites at the surface or those at the interior of the nanocrystals. There have been many reports on studies of the site symmetry of activators of the rare-earth-doped nanocrystals,[27,30–33] while the corresponding systematic research on m- and t-$LaVO_4$:Eu nanocrystals has not been achieved. In this work, the different Eu^{3+} sites in the nanocrystals were selectively excited with a tunable dye laser and the luminescence spectra of each site were recorded separately.

Lattice Site of the m-$LaVO_4$:Eu Nanocrystals and of the Bulk Material

To compare the site symmetry of the dopant ions in the bulk material and in the nanocrystals, site-selective spectra of the m-$LaVO_4$:Eu (3 mol-%) nanocrystals and the bulk material were studied. The above results show that for emission with an excitation wavelength of 310 nm, the spectra for bulk m-$LaVO_4$:Eu is much more resolved. We further investigated the luminescence spectra under an excitation wavelength of 355 nm for this wavelength is located at the low-energy edge of the absorption band of the vanadate groups (see Figure 7b), and the emission excited at this wavelength should be more sensitive as less Eu^{3+} is excited. Figure 11a shows the $^5D_0$–$^7F_2$ transition excited at 355 nm at 77 K, and this process is quite different from that of the bulk. Besides the peaks located at 612.4 and 616.2 nm, another peak at 621.2 nm is also observed for the m-$LaVO_4$:Eu nanocrystals. Figure 11b shows the excitation spectra of the m-$LaVO_4$:Eu (3 mol-%) nanocrystals and the bulk material by monitoring the transition of $^5D_0$–$^7F_2$. For the bulk material, only one peak located at 578.7 nm appears. For the nanocrystals, an extra peak at 580.7 nm appears. The above results suggest there is a new site in the nanocrystals. The peak centered at 578.7 nm, which is the same for the bulk as for the nanocrystal spectra, should come from an intrinsic Eu^{3+} site in m-$LaVO_4$:Eu (C_1 point group, site 1-m). The peak centered at 580.7 nm in the spectra of the nanocrystals is related to the Eu^{3+} ions in a new site (site 2-m), which is not observed in the bulk spectra.

The site-selective emission spectra (Figure 11c) of the transition $^5D_0$–$^7F_2$ were recorded under excitations at 578.7 and 580.7 nm for the nanocrystals and at 578.7 nm for the bulk material. The emission spectrum of the bulk consists of four peaks that likely originate from site 1-m. For the nanocrystals, the same emission behavior is observed as that in the bulk with excitation at 578.7 nm, while a different emission behavior is observed, with two prominent peaks at 614.0 and 621.2 nm, when excited at 580.7 nm. This indicates that excitation at 580.7 nm corresponds to a new site, named site 2-m, and it is obvious that only the new site induces the difference observed for the $^5D_0$–$^7F_2$ transition for the bulk material and the nanocrystals. For the m-$LaVO_4$:Eu nanocrystals with higher Eu content, such as the m-$LaVO_4$:Eu (12 mol-%) nanocrystals, site-selective spectra were also recorded (Figure S6). Similarly, two kinds of Eu^{3+} sites could be identified in the m-$LaVO_4$:Eu (12 mol-%) nanocrystals, which is the same as those of the m-$LaVO_4$:Eu nanocrystals with lower doping concentrations. From the site-selective spectra, it is apparent that the appearance of site 2-m is independent of the content of dopant (i.e. the Eu^{3+} ions).

There have been some reports on the new sites of Eu^{3+} in YBO_3:Eu,[27] $LaPO_4$:Eu,[30,32] YVO_4:Eu,[31] and LaF_3:Eu[33] nanocrystals. Most of the dopant ions occupy the same lattice site as that in the bulk (bulk site), and the rest occupy other sites, named as surface sites in general, which result from the increase in the surface area and surface lattice distortion. For m-$LaVO_4$:Eu nanocrystals, considering that m-$LaVO_4$ and $EuVO_4$ are not isostructural materials, very few traces of $EuVO_4$ may coexist with m-$LaVO_4$:Eu and induce the new site (site 2-m). This possibility is completely excluded by careful comparison and analysis of the site-selective spectra of the m-$LaVO_4$:Eu nanocrystals and those of the pure $EuVO_4$ nanocrystals (Figure S7). The emission from site 2-m is quite different from the emission in the site-selective spectra of the $EuVO_4$ nanocrystals. Therefore, site

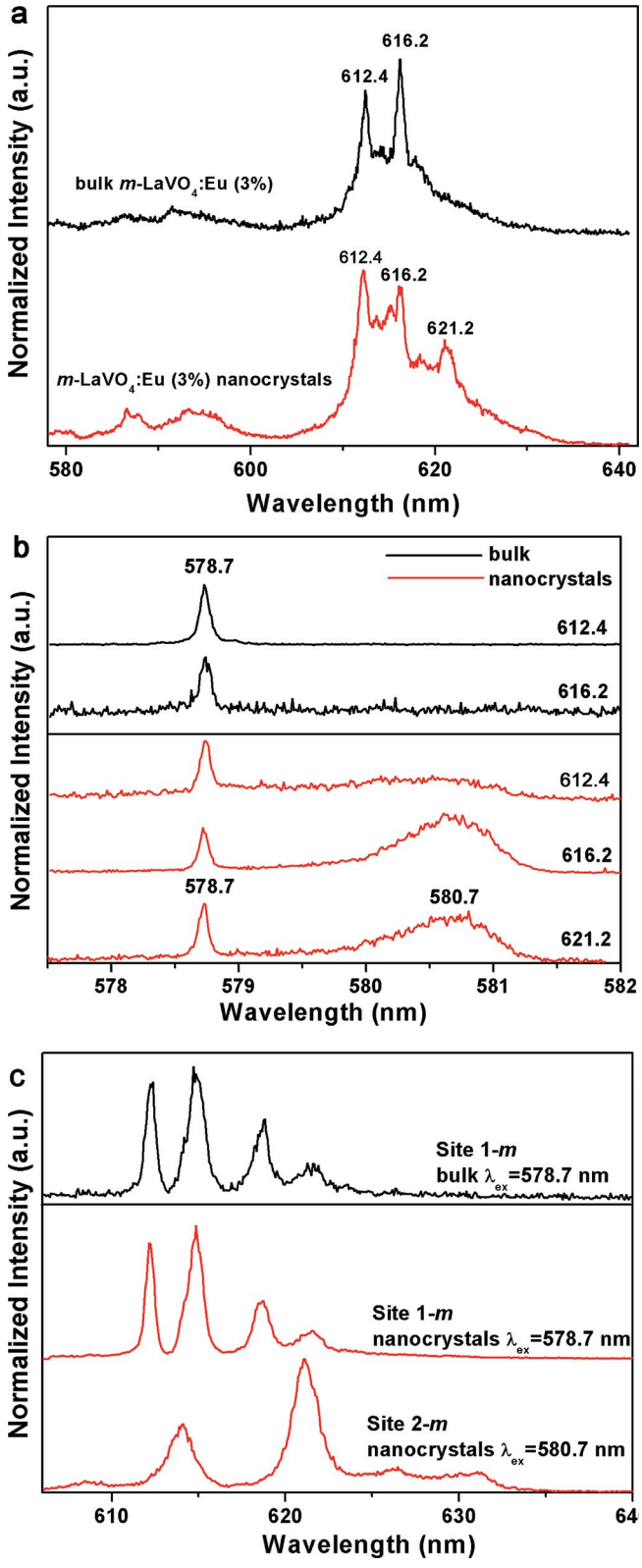

Figure 11. (a) High-resolution emission spectra of the bulk and nanocrystals of m-$LaVO_4$:Eu (3 mol-%) under 355 nm excitation. (b) Excitation spectra monitoring the $5D_0$–$7F_2$ transition for the bulk (at 612.4 and 616.2 nm) and for the nanocrystals (at 612.4, 616.2, and 621.2 nm). (c) Site-selective emission spectra of the m-$LaVO_4$:Eu (3 mol-%) nanocrystals and the bulk material excited at 578.7 and 580.7 nm, respectively.

2-m in the m-$LaVO_4$:Eu nanocrystals does not belong to the Eu^{3+} ions in the $EuVO_4$ nanocrystals. Considering the size of the nanocrystals and the site-selective spectra, it is reasonable to conclude that site 2-m originates from the Eu^{3+} ions located at the surface of the m-$LaVO_4$:Eu nanocrystals. It is a kind of surface state related lattice site.

Lattice Site of Eu^{3+} in the t-$LaVO_4$:Eu Nanocrystals

In order to get a full view of the site symmetry of Eu^{3+} in the t-$LaVO_4$:Eu nanocrystals, the site-selective spectra of both the t-$LaVO_4$:Eu (10 mol-%) nanocrystals and the corresponding quasi-bulk material were investigated. The quasi-bulk material of t-$LaVO_4$:Eu was prepared by annealing the t-$LaVO_4$:Eu (10 mol-%) nanocrystals at 800 °C for 6 h. The XRD pattern (Figure S8) of the quasi-bulk material sharpened but still denotes the zircon–type structure without any monazite-type diffraction peaks, which is in accordance with our previous results.[17] The high-resolution emission spectra of the t-$LaVO_4$:Eu nanocrystals and the quasi-bulk material under 355 nm excitation at 77 K are shown in Figure 12a. Both of the emission spectra consist of two groups of emissions between 580 and 640 nm, which can be attributed to $^5D_0$–$^7F_1$ and $^5D_0$–$^7F_2$ transitions of Eu^{3+}, respectively. For the $^5D_0$–$^7F_2$ transition at 613.8 and 618.2 nm, the intensity ratio ($I_{613.8}/I_{618.2}$) is different between the nanocrystals and the quasi-bulk material. Figure 12b shows the excitation spectra by monitoring the emission at 618.2 nm. For the quasi-bulk material of t-$LaVO_4$:Eu, there is only one peak centered at 580.6 nm. While for the nanocrystals, besides the main peak at 580.6 nm, there is also a satellite peak centered at 581.0 nm. Therefore, there is only one site that exists in quasi-bulk t-$LaVO_4$:Eu, while perhaps two sites exist in the nanocrystals. The peak centered at 580.6 nm in the excitation spectra of both the quasi-bulk material and the nanocrystals should originate from the intrinsic Eu^{3+} site in t-$LaVO_4$:Eu, which corresponds to a D_{2d} (site 1-t) symmetry. The peak centered at 581.0 nm for the nanocrystals may be related to the Eu^{3+} ions from a different site (site 2-t).

The site-selective spectra are shown in Figure 12c. The emission spectra excited at 580.6 nm for both the quasi-bulk material and the nanocrystals of t-$LaVO_4$:Eu is almost the same with two main peaks for the $^5D_0$–$^7F_2$ transition, which should originate from the Eu^{3+} ions in the interior of the nanocrystals (site 1-t). The emission with an excitation wavelength of 581.0 nm indicates a different lattice site of Eu^{3+}, and this is confirmed by the decay of the emissions from these different sites. Figure 12d shows the decay curve for $^5D_0$–$^7F_2$ for site 1-t and site 2-t for the t-$LaVO_4$:Eu nanocrystals, and the lifetimes are 1.1 ms and 0.86 ms, respectively. The emission from site 1-t exhibits a relatively longer lifetime than that of site 2-t. Nonradiative transition paths, such as those involving the hydroxy groups or the quenching centers, will shorten the lifetime of the excited states, and thus lower the emission intensity. For the nanosized materials, the high surface-to-volume ratio induces the transition from the surface or surface-related sites exhibit a relatively fast process.[34] By considering the size dimension,

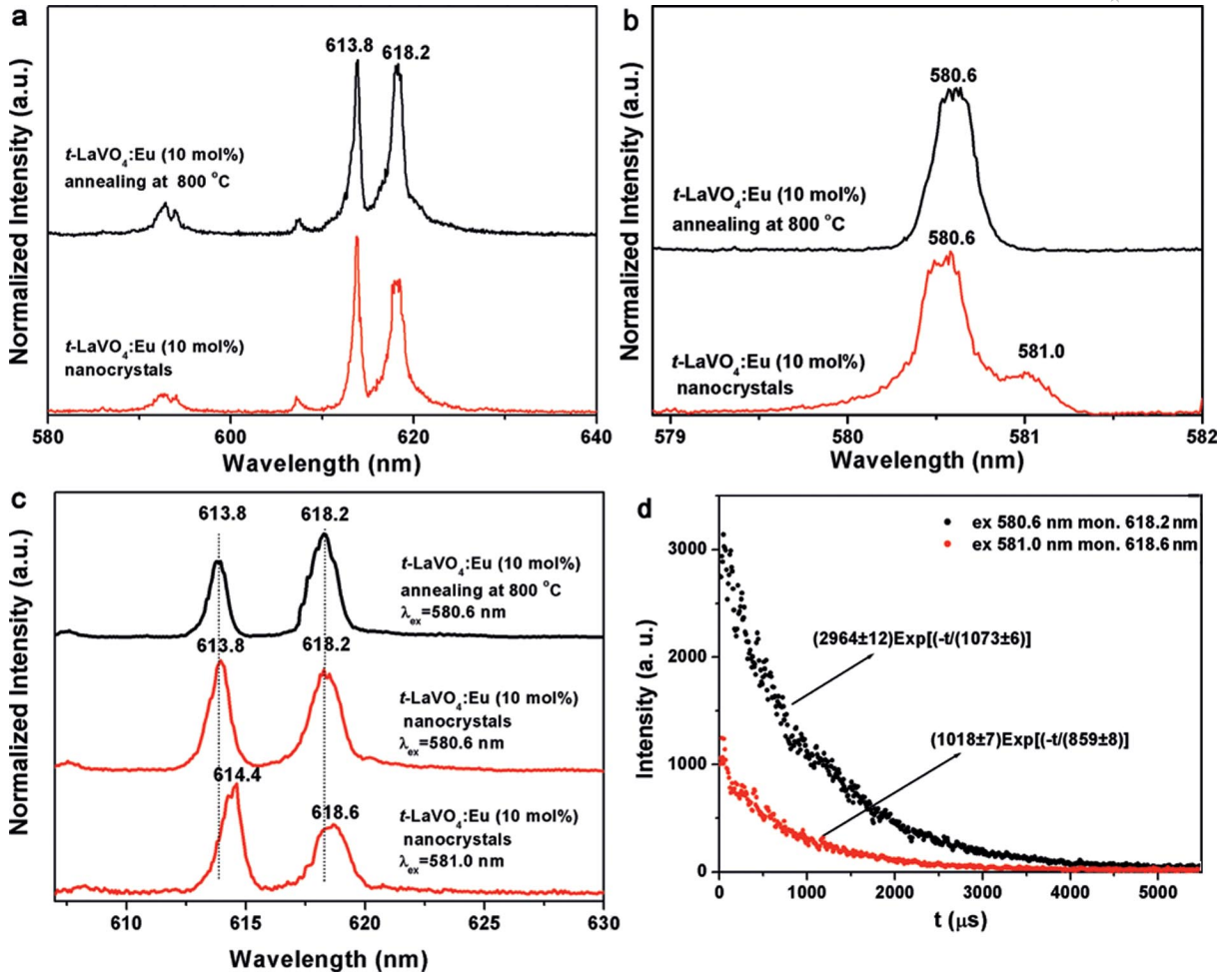

Figure 12. (a) High-resolution emission spectra of the quasi-bulk material and of the nanocrystals of t-$LaVO_4$:Eu (10 mol-%) under 355 nm UV excitation. (b) Excitation spectra monitoring the $5D_0$–$7F_2$ transition (at 618.2 nm) for the quasi-bulk material and the nanocrystals. (c) Emission spectra of the t-$LaVO_4$:Eu quasi-bulk material and of the nanocrystals excited at 580.6 and 581.0 nm, respectively. (d) Decay curves of the $5D_0$–$7F_2$ emission by exciting site 1-t and site 2-t for the t-$LaVO_4$:Eu (10 mol-%) nanocrystals.

it is reasonable to conclude that the site 2-t of the t-$LaVO_4$:Eu nanocrystals with shorter lifetimes should originate from Eu^{3+} located at or near the surface of the t-$LaVO_4$:Eu nanocrystals.[31]

On the basis of the above discussions, for both m- and t-$LaVO_4$:Eu nanocrystals, the Eu^{3+} ions occupy two types of sites. One is the interior site, which is the same as that of the bulk, and the other is a new site that comes from the surface states. The distribution of Eu^{3+} in these two sites is illustrated in Scheme 1. The contribution of these sites to the emission is correlated with the dimension of the nanocrystals. It is expected that with a decrease in the particle size, the surface sites will have a greater impact on the emission behavior because of the relatively large amount of Eu^{3+} ions located at or near the surface. Similarly, a higher Eu^{3+} content may also induce more Eu^{3+} ions located at the surfaces of the nanocrystals, and its effect on the luminescence behavior will be more significant, as can be seen from Figure S6, in which the emission at 621.2 nm for m-$LaVO_4$:Eu (12 mol-%) is stronger than that of the m-$LaVO_4$:Eu (3 mol-%) nanocrystals (Figure 10a). These site-related emission spectra are important not only for straightforward microprobe or microstructure studies, but also for constructing luminescence materials with different spectroscopic properties.

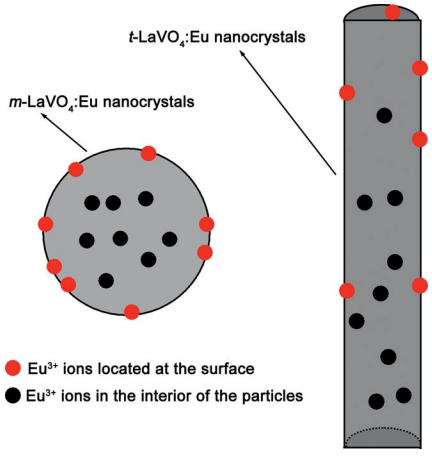

Scheme 1. Illustration of the Eu^{3+} site related to its distribution in the m- and t-$LaVO_4$:Eu nanocrystals.

Conclusions

Pure m- and t-$LaVO_4$:Eu nanocrystals were selectively prepared by citric anion- and by EDTA-assisted hydrothermal methods, respectively, and the luminescence properties of the m- and t-$LaVO_4$:Eu nanocrystals were investigated. Relative to m-$LaVO_4$, t-$LaVO_4$ is a more suitable host for the Eu^{3+} ion activators. Meanwhile, t-$LaVO_4$:Eu nanocrystals provide a new and cheap candidate for luminescence materials with potential applications in lighting, displays, and biological detection. In addition to structural characterization, the Eu^{3+} sites in the nanocrystals were identified by site-selective spectroscopy studies. The results show that for both the m- and t-$LaVO_4$:Eu nanocrystals, the Eu^{3+} ions occupy two types of sites. One site is the same as that of the bulk, and the other is a surface site. The structurally controlled synthesis of the m- and t-$LaVO_4$:Eu nanocrystals and the spectroscopic identification of the Eu^{3+} sites provide important experimental evidence for the rare earth luminescence spectroscopy study. Furthermore, the correlation between the microstructure and luminescence behavior was explored for the design and synthesis of novel luminescence materials.

Experimental Section

Synthesis

m-$LaVO_4$:Eu Nanocrystals: In the preparation procedure of the m-$LaVO_4$:Eu nanocrystals, an appropriate amount of a mixed solution consisting of rare earth nitrate [$La(NO_3)_3$+$Eu(NO_3)_3$] (0.0016 mol) with a fixed molar ratio of Eu/La, sodium orthovanadate ($Na_3VO_4 \cdot 12H_2O$, 0.640 g, 0.0016 mol), sodium citrate ($Na_3C_6O_7H_5 \cdot 2H_2O$, 1.41 g, 0.0048 mol), and distilled water was vigorously magnetically stirred. The pH value of the mixture was adjusted to 10 by the addition of 3 mol/L nitric acid (HNO_3) or sodium hydroxide (NaOH) solution, and the final volume of the mixture was kept as 80 mL. After stirring for ten minutes, the mixture was transferred into a Teflon-lined stainless steel autoclave with a capacity of 100 mL for hydrothermal treatment at 180 °C for 24 h. As the autoclave cooled down to room temperature naturally, the precipitation was separated by centrifugation, washed with distilled water and absolute ethanol, and dried under vacuum at 80 °C.

t-$LaVO_4$:Eu Nanocrystals and $EuVO_4$ Nanocrystals: The synthesis of the t-$LaVO_4$:Eu nanocrystals is similar to that of the m-$LaVO_4$:Eu nanocrystals. To obtain the pure t-$LaVO_4$:Eu nanocrystals, ethylenediaminetetraacetic acid (EDTA) instead of sodium citrate was added as an additive, the molar ratio of [EDTA]/[La^{3+}, Eu^{3+}] was 1:12. The $EuVO_4$ nanocrystals were prepared through a similar route, with the exception that the ratio of [EDTA]/[Eu^{3+}] was kept at 0.5.

Bulk $LaVO_4$:Eu: For comparison, bulk $LaVO_4$:Eu was prepared by direct solid-state reaction with a certain amount of La_2O_3, Eu_2O_3 (>99.99%) and NH_4VO_3 as starting materials. Typically, for the synthesis of bulk m-$LaVO_4$:Eu with 1 mol-% Eu content, La_2O_3 (1 g), Eu_2O_3 (11 mg), and NH_4VO_3 (0.73 g) were milled with the addition of ethanol (10 mL) for 30 min. The slurry was then dried at 80 °C for 2 h to remove the ethanol and calcinated at 1200 °C for 6 h.

Characterization: The powder X-ray diffraction (XRD) patterns were recorded on a Rigaku D/max-2000 diffractometer by using Cu-K_α radiation (λ = 1.5418 Å). Transmission electron microscopy (TEM) images were taken on a JEOL 200CX transmission electron microscope under a working voltage of 160 kV. High-resolution TEM (HRTEM) characterizations were performed with a Philips Tecnai F30 FEG-TEM operated at 300 kV. The samples were supported on carbon-coated copper grids by dropping the ethanol suspension containing uniformly dispersed nanocrystals. Raman spectra were determined on a Horiba Jobin Yvon LabRam HR 800 spectrometer equipped with a grating of 2400 grooves/mm, Olympus BX41 microscope (50× objective lens) and charged-coupled device detector. The spectra were excited with the 488 nm line of an Ar^+ laser, backscattering geometry was adopted for the measurement with a laser power of 30 mW. Fluorescence spectra were recorded on a Hitachi F-4500 spectrophotometer equipped with a 150 W Xe-arc lamp at room temperature. Quantum yields were determined by comparing the integrated emission of the nanocrystal ethanol suspension and a Rhodamine B ethanol solution, with the same optical density (OD < 0.1) and excited at the same wavelength (310 nm). High-resolution fluorescence spectra were measured at 77 K under 355-nm excitation provided by a YAG:Nd laser with a third-harmonic generator, the signal was collected with a SPEX1403 double-grating monochromator and a R955 photomultiplier. Site-selective excitation was performed by the same set of apparatus with a YAG:Nd (532 nm) pumped Rhodamine 6G dye laser and a boxcar averager.

Supporting Information (see footnote on the first page of this article): Unit cell parameters for the m-$La_{1-x}VO_4$:Eu_x and t-$La_{1-x}VO_4$:Eu_x nanocrystals, graphs for the unit cell parameters vs. Eu^{3+} content for the m-$LaVO_4$:Eu and t-$LaVO_4$:Eu nanocrystals, XRD patterns and TEM images of the $EuVO_4$ nanocrystals and of bulk $LaVO_4$:Eu, emission intensity vs. Eu^{3+} content of the t-$LaVO_4$:Eu nanocrystals, high-resolution emission spectra of the m-$LaVO_4$:Eu nanocrystals, excitation spectra of the transition of $^5D_0$–$^7F_2$ for the m-$LaVO_4$:Eu nanocrystals, high-resolution emission and excitation spectra of $EuVO_4$ nanocrystals, and XRD patterns of the quasi-bulk material are presented.

Acknowledgments

This work was supported by the National Basic Research Program of China (973 Program, 2006CB601104) and the Natural Science Foundation of China (NSFC, 20971005, 20821091, and 20931160429).

[1] K. Riwotzki, H. Meyssamy, H. Schnablegger, A. Kornowski, M. Haase, *Angew. Chem. Int. Ed.* **2001**, *40*, 573–576.
[2] J. C. Park, H. K. Moon, D. K. Kim, S. H. Byeon, B. C. Kim, K. S. Suh, *Appl. Phys. Lett.* **2000**, *77*, 2162–2164.
[3] J. R. O'Connor, *Appl. Phys. Lett.* **1966**, *9*, 407–409.
[4] D. B. Barber, C. R. Pollock, L. L. Beecroft, C. K. Ober, *Opt. Lett.* **1997**, *22*, 1247–1249.
[5] G. S. Yi, H. C. Lu, S. Y. Zhao, G. Yue, W. J. Yang, D. P. Chen, L. H. Guo, *Nano Lett.* **2004**, *4*, 2191–2196.
[6] D. K. Williams, B. Bihari, B. M. Tissue, *J. Phys. Chem. B* **1998**, *102*, 916–920.
[7] X. C. Jiang, C. H. Yan, L. D. Sun, Z. G. Wei, C. S. Liao, *J. Solid State Chem.* **2003**, *175*, 245–251.
[8] S. Faria, E. J. Mehalchick, *J. Electrochem. Soc.* **1974**, *121*, 305–307.
[9] Z. M. Fang, Q. Hong, Z. H. Zhou, S. J. Dai, W. Z. Weng, H. L. Wan, *Catal. Lett.* **1999**, *61*, 39–44.
[10] M. Ross, *IEEE J. Quantum Electron.* **1975**, *11*, 938–939.

[11] A. K. Levine, F. C. Palilla, *Appl. Phys. Lett.* **1964**, *5*, 118–1120.
[12] H. Fuess, A. Kallel, *J. Solid State Chem.* **1972**, *5*, 11–14.
[13] C. E. Rice, W. R. Robinson, *Acta Crystallogr., Sect. B* **1976**, *32*, 2232–2233.
[14] B. C. Chakoumakos, M. M. Abraham, L. A. Boatner, *J. Solid State Chem.* **1994**, *109*, 197–202.
[15] R. C. Ropp, B. Carroll, *J. Inorg. Nucl. Chem.* **1973**, *35*, 1153–1157.
[16] Y. Oka, T. Yao, N. Yamamoto, *J. Solid State Chem.* **2000**, *152*, 486–491.
[17] C. J. Jia, L. D. Sun, L. P. You, X. C. Jiang, F. Luo, Y. C. Pang, C. H. Yan, *J. Phys. Chem. B* **2005**, *109*, 3284–3290.
[18] C. J. Jia, L. D. Sun, F. Luo, X. C. Jiang, L. H. Wei, C. H. Yan, *Appl. Phys. Lett.* **2004**, *84*, 5305–5307.
[19] J. F. Liu, Y. D. Li, *Adv. Mater.* **2007**, *19*, 1118–1122.
[20] E. Antic-Fidancev, J. Hölsä, M. Lemaitre-Blaise, P. Porcher, *J. Phys.: Condes. Matter* **1991**, *3*, 6829–6843.
[21] U. Rambabu, D. P. Amalnerkar, B. B. Kale, S. Buddhudu, *Mater. Res. Bull.* **2000**, *35*, 929–936.
[22] M. Yu, J. Lin, S. B. Wang, *Appl. Phys. A-Mater. Sci. Pro.* **2005**, *80*, 353–360.
[23] J. W. Stouwdam, M. Raudsepp, F. C. J. M. van Veggel, *Langmuir* **2005**, *21*, 7003–7008.
[24] R. D. Shannon, *Acta Crystallogr., Sect. A* **1976**, *32*, 751–767.
[25] B. R. Judd, *Phys. Rev.* **1962**, *127*, 750–761.
[26] G. S. J. Ofelt, *Chem. Phys.* **1962**, *37*, 511–520.
[27] Z. G. Wei, L. D. Sun, C. S. Liao, J. L. Yin, X. C. Jiang, C. H. Yan, S. Z. Lu, *J. Phys. Chem. B* **2002**, *106*, 10610–10617.
[28] L. G. Van Uitert, L. F. Johnson, *J. Chem. Phys.* **1966**, *44*, 3514–3522.
[29] G. Blasse, *J. Chem. Phys.* **1966**, *45*, 2356–2360.
[30] O. Lehmann, K. Kömpe, M. Haase, *J. Am. Chem. Soc.* **2004**, *126*, 14935–14942.
[31] C. H. Yan, L. D. Sun, C. S. Liao, Y. X. Zhang, Y. Q. Lu, S. H. Huang, S. Z. Lü, *Appl. Phys. Lett.* **2003**, *82*, 3511–3513.
[32] H. W. Song, L. X. Yu, S. Z. Lü, T. Wang, Z. X. Liu, L. M. Yang, *Appl. Phys. Lett.* **2004**, *85*, 470–472.
[33] V. Sudarsan, F. C. J. M. van Veggel, R. A. Herring, M. Raudsepp, *J. Mater. Chem.* **2005**, *15*, 1332–1342.
[34] R. S. Meltzer, S. P. Feofilov, B. Tissue, H. B. Yuan, *Phys. Rev. B* **1999**, *60*, R14012–R14015.

Received: January 16, 2010
Published Online: April 14, 2010

